NASA CR-66120

A Study Of Man's Physical Capabilities On The Moon

VOLUME IV

INVESTIGATION OF LUNAR GRAVITY SIMULATION TECHNIQUES

By A.J. Bartley, R.P. Hess, R.J. Kirschensteiner,
D.A. Millett, R.J. Morgen and J.B. Reswick

Prepared under Contract No. NAS 1-4449 by
CASE INSTITUTE OF TECHNOLOGY
ENGINEERING DESIGN CENTER
University Circle
Cleveland, Ohio

for

NATIONAL AERONAUTICS AND SPACE ADMINISTRATION

NASA CR-66120

A Study Of Man's Physical Capabilities On The Moon

VOLUME IV

INVESTIGATION OF LUNAR GRAVITY SIMULATION TECHNIQUES

By A.J. Bartley, R.P. Hess, R.J. Kirschensteiner,
D.A. Millett, R.J. Morgen and J.B. Reswick

Prepared under Contract No. NAS 1-4449 by
CASE INSTITUTE OF TECHNOLOGY
ENGINEERING DESIGN CENTER
University Circle
Cleveland, Ohio

for

NATIONAL AERONAUTICS AND SPACE ADMINISTRATION

A STUDY OF MAN'S PHYSICAL CAPABILITIES

ON THE MOON

ABSTRACT

A study was made to compare man's energy expenditure and gait characteristics, during self locomotion at various rates, in earth and in simulated lunar gravity conditions. The tests were made for the subject walking and running on the level and on grades up to 30° while in shirt sleeves and while wearing a suit pressurized to 3.5 psig. The results, presented in four volumes, may be useful for the design of space suits and life support systems and the planning of lunar exploration missions and their logistics.

FOREWORD

This volume covers the investigation of lunar gravity simulation techniques in "A Study of Man's Physical Capabilities on the Moon", NASA Contract NAS 1-4449. The prime contract was administered by Langley Research Center, with Mr. William Letko serving as NASA Technical Monitor.

The investigation was performed by Case Institute of Technology under subcontract to Northrop Space Laboratories where Dr. Walter Kuehnegger served as the Principal Investigator. Professor James B. Reswick, Director of the Case Institute engineering design center, guided and directed the investigation. The Cleveland Institute of Art provided extensive assistance to the Case Institute by fabricating the body harness and counterbalance suspension system, as directed by Professor Roy P. Hess.

In view of the complexity and scope of the work performed under this contract, the final report has been organized in four separate volumes (numbered I thru IV). Since the work itself was broken down into phases it was possible to treat each phase individually and document them correspondingly. The four volumes which comprise this report are identified as follows.

CR-66115 Volume I, Part 1 - Lunar Gravity Simulation Facility

CR-66116 Volume I, Part 2 - Instrumentation

CR-66117 Volume II - Part 1 - Biomechanics Research Program

CR-66118 Volume II - Part 2 - Biomechanics Research Program Appendices

CR-66119 Volume III - Work Physiology Research Program

CR-66120 Volume IV - Investigation of Lunar Gravity Simulation Techniques

Volumes I thru III were produced by NSL and have been assigned Northrop Space Laboratories' document number NSL 65-153. Volume IV was prepared from material contributed by Case Institute and reports on their portion of the contract effort. The total report (all four volumes) summarizes the performance during the contract period from 2 November 1964 to 30 September 1966.

CONTENTS

PRECEDING PAGE BLANK NOT FILMED.

ILLUSTRATIONS

VOLUME IV - INVESTIGATION OF LUNAR GRAVITY SIMULATION TECHNIQUES

By A. J. Bartley, R. P. Hess, R. J. Kirschensteiner,
D. A. Millett, R. J. Morgen and J. B. Reswick

Case Institute of Technology
Engineering Design Center

SUMMARY

The opening sections of the report are concerned with the inclined plane method of simulating lunar gravity and some attempt has been made to improve the versatility of this method by refining the harness design.

The bulk of the report deals with the development of a new method of simulating lunar gravity in which it is proposed to suspend the test subject in marionette-like fashion from a steel ceiling. A new concept of a magnetic air pad was used as the support at roof level and this enabled the subject to move freely with minimal frictional resistance. Negator springs were used to nullify five-sixths of the subject's weight.

The practicality of the system has been proved by building a 1/6 scale working model. A full-size system has not yet been built but sufficient research and design data has been collected to enable this to be done.

INTRODUCTION

In a previous report to Northrop the authors put forward a collection of new ideas in the field of lunar gravity simulation. The subject matter ranged over a wide field being concerned with body suspension systems, limb assist mechanisms, lunar topography simulation and improvements to the inclined plane type of simulator. In addition, a number of ideas were put forward with a view to developing some form of "vertical suspension" simulator which would be complementary to existing inclined plane techniques and which would enable the test subject to perform maneuvers which are difficult or impossible to execute on the inclined plane.

The final report is concerned with the practical exploitation of some of the more promising ideas in the previous report. The new work can be broadly divided into three sections:

(1) Improvements for the inclined plane simulator

(2) Design and development of a vertical suspension system

(3) Design and development of body harness and limb support mechanisms

In Section (1), the emphasis has been placed on the construction of a suspension system and harness which would give the test subject more freedom of movement than has been possible hitherto.

In Section (2) consideration is given to the problem of developing a system in which the test subject would be suspended vertically from the ceiling of a room and yet be free to move in any direction within the confines of the room. The proposed solution involves the use of negator springs to give the desired uplift to the test subject and a magnetic-air type ceiling attachment to give the required mobile support at roof level.

Finally, in Section (3) the design of harnesses and limb assist devices is considered. This work has been done in connection with the vertical suspension system based on the magnetic air-pad and negator spring device.

SECTION 1

IMPROVEMENTS FOR THE INCLINED PLANE SIMULATOR

A number of improvements were applied to the Langley type inclined plane simulator (Ref 1) and these are illustrated in Figure 1.

Lateral Movement of the Legs

The support devices for the legs were attached to the same cable which went from each leg support up and over a pulley. This pulley was attached to the spreader bar which held the cables to all the supports for the body segments.

This arrangement allowed the subject to spread and pull together his legs thereby achieving a more natural standing, walking, etc., situation. Because of the mechanical arrangement of the cable and pulley the legs had to spread and pull together in unison; however, this duplicates normal leg action and was found to be a desirable feature, even though there was no need for a wide stance to maintain balance when landing from a jump, etc.

Rotation of the Head

A cable passing from a point on the front of the helmet at approximately the midpoint of the forehead and thence up and over a pulley to a point in the middle of the back of the helmet allowed azimuthal rotation of the head. No important actual area of freedom was introduced with this device; however, it did cause the subject to feel less contained by the entire apparatus and consequently was considered to be a plus feature.

Upper Arm Freedom of Swing

A relatively large "C" brace was fabricated and its lower horizontal extension was attached to the upper body harness. The cable support to the spreader bar was attached to the upper horizontal extension of this "C" brace. This "C" brace replaced the cable which went directly from the upper body harness to the spreader bar, and in so doing eliminated cable interference when the upper arm was placed along side the body in a hanging down position or when the arm was swung backwards. Again no important functional freedom was introduced but the removal of another constraint was considered to be a plus factor by various subjects who tried the system with and without this innovation.

Notes on the Development of an Additional Important Freedom of Movement for the Inclined Plane Simulator

The freedom of rotation around the subject's Z axis (Figure 2) seemed to be an important one to incorporate for it would allow the subject to turn round and re-trace his steps as and when he liked.

As a result, thought was given to this problem and the resulting best solution indicated that two additional "C" braces extending in front of the subject would be required. One "C" brace would attach to the hip and chest supports and the other would attach to the present sling supported leg.

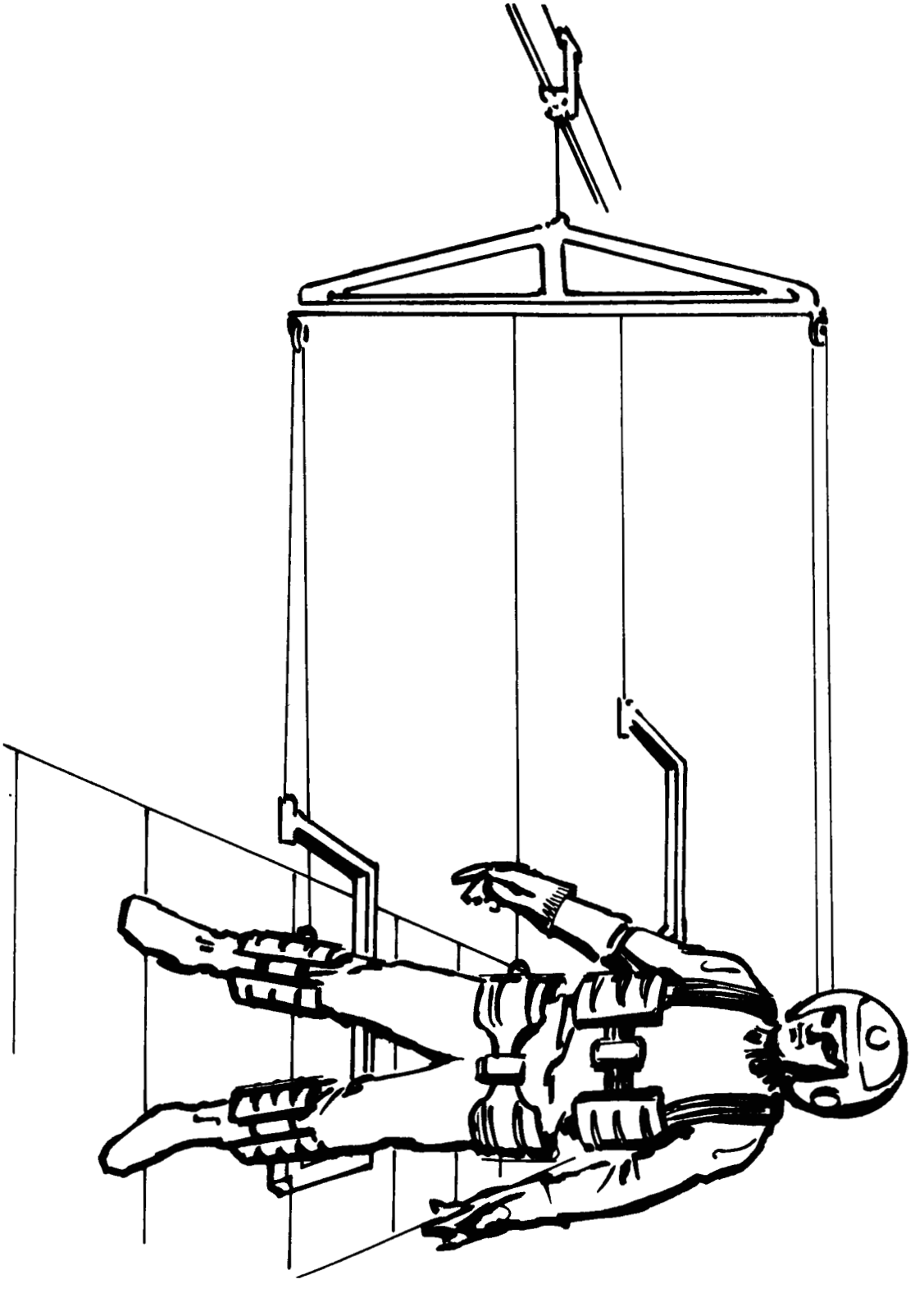

Figure 1. - Inclined plane simulator improvements

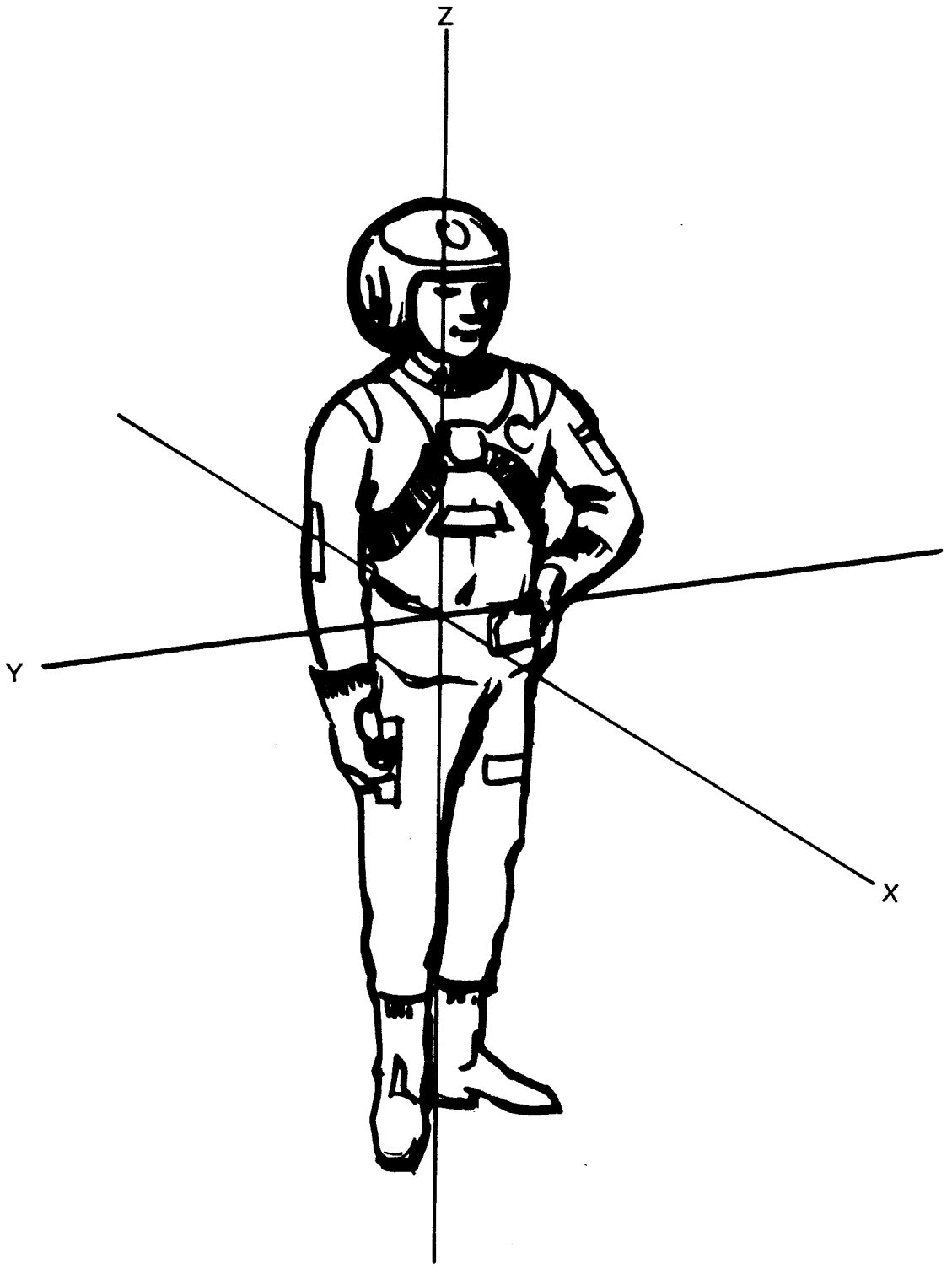

Figure 2. - Subject axis system

It was decided not to modify the existing equipment to include these additional "C" braces because there are a number of disadvantages associated with their presence. Among these are:

1. The mechanism and bulk of two additional "C" braces in front of the subject appeared as if it would be psychologically inhibiting with regard to a sense of freedom on the part of the subject.

2. The "C" braces extending in front of the subject would interfere with many crawling or bending movements.

However, in order to obtain maximum versatility, it may be desirable to design future inclined plane simulators in a manner that would permit easy addition and removal of these extra braces.

Inclined Plane System - Conclusions

By suitable development and refinement, it is possible to build an inclined plane simulator which would give the test subject four + degrees of freedom and also provide him with a reasonably large test area in which to work. The experiments carried out so far have shown that it is possible to crawl, walk, run and jump with relative ease. In view of the simplicity of the apparatus the results were quite promising and there would appear to be little doubt that this type of simulator merits further development.

Nevertheless, the inclined plane methods possess certain limitations. One of these is the lack of realism felt by the test subject who cannot completely ignore the fact that he is attempting to walk on a near-vertical wall instead of on the floor when using a short cable radius. This disadvantage can no doubt be partially overcome by suitable topographical design and psychological conditioning of the subject.

Another disadvantage is the difficulty of achieving movement along the subject's X axis which is almost vertical relative to earth. Assuming, as suggested previously, that it would be possible with relative ease to give the subject azimuthal rotation of at least 180° it would still be difficult to provide freedom of movement in the X direction because his weight would need to be counterbalanced with great precision to nullify the effects of one g earth gravity.

For these and other reasons it was considered desirable to examine the practical possibilities of vertical suspension systems, and the work presented in the next section will provide some idea of the progress made in this field.

SECTION 2

DESIGN AND DEVELOPMENT OF VERTICAL SUSPENSION SYSTEM

In any type of lunar gravity simulator there are two major problems to be solved - namely, how to reduce the weight of the subject, and how to provide him with the maximum amount of mobility. These two problems are interdependent to the extent that a solution to the one will usually limit the number of possible solutions to the other.

In the vertical simulator now discussed, the aim was to suspend the test subject from the ceiling of a large room in such a way that he was able to move freely in any direction he chose by using a suspension system which incorporated a negator spring device and a magnetic air pad. Figure 3 gives some idea of the kind of system envisaged.

A Negator Spring System

There are two types of negator spring units, both employing the same basic negator spring coil. These are the simple extension spring and the constant torque motor.

The force obtained by unwinding a negator coil is almost perfectly constant (i.e., force - deflection gradient is zero). Through various methods of manufacturing control, gradients ranging from slightly positive to slightly negative can be achieved.

A dynamic analysis of the proposed system (see appendix - A) indicates that a negator having a slightly positive force - deflection gradient is desirable. The reason for this is that as the negator coil is unwound, an increasing force must be exerted to overcome the weight of the extended portion.

The practical work on negator spring units has been confined so far to the design and manufacture of a 5/6 g negator unit for the prototype model shown in Figure 4. This consists of two simple coil springs mounted back-to-back to provide an uplift of 20 lb. over a displacement range of 30 inches.

Generally it is considered that negator spring devices are well suited to lunar gravity simulator applications because of the many advantages they offer. These include:

1. Constant force for large deflections.
2. Low weight and compactness.
3. Relatively low inertial effects compared with counter balance weight systems.
4. Relatively little friction since there is no friction inherent in the spring.

Magnetic Air Pad Development

The magnetic air pad was an overhead support fixture. This device gave the supported object three degrees of freedom. The first two degrees of freedom were horizontal translation in a plane parallel to the ceiling. The third degree of freedom was

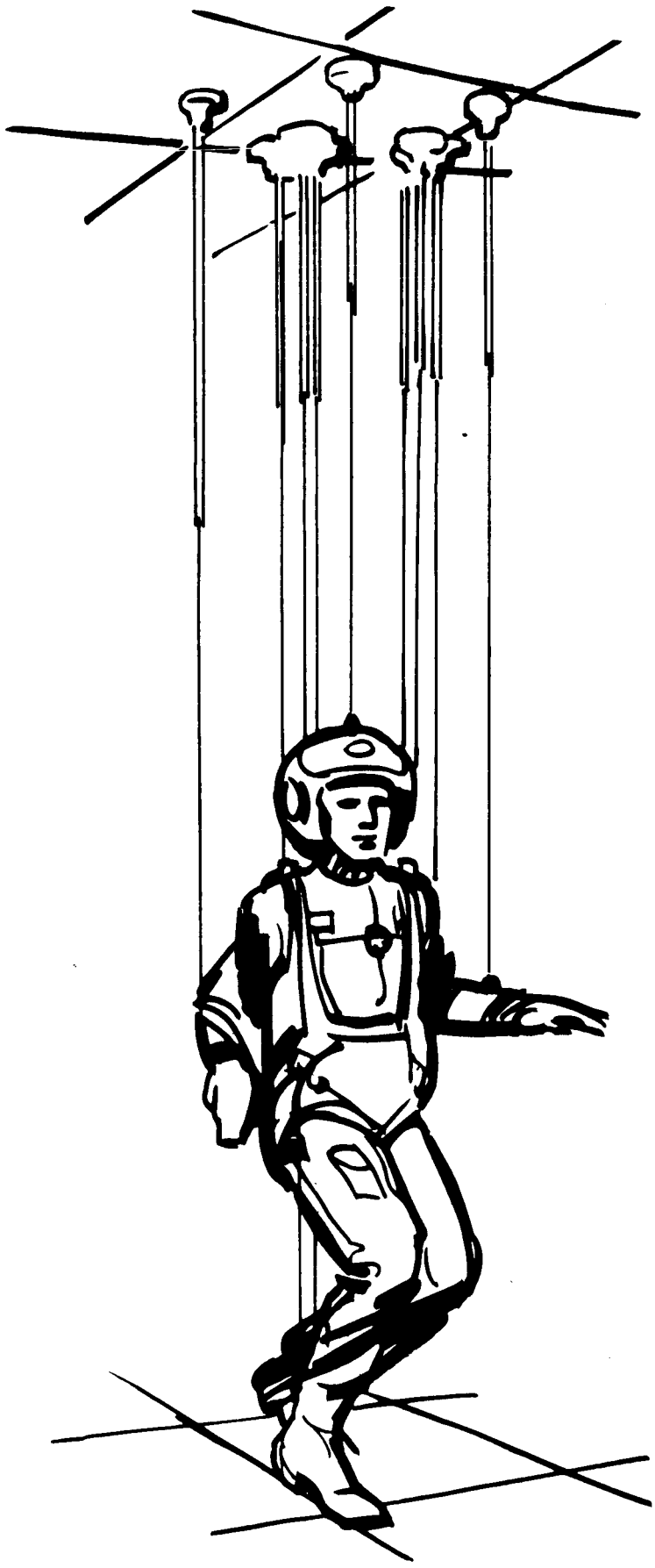

Figure 3. - Vertical suspension simulator

Figure 4. - Vertical suspension simulator, prototype model

rotation, either clockwise or counterclockwise. These various movements were obtained with almost negligible friction.

The device was structurally simple. It consisted of a flat disc with an air orifice at its center. Around the orifice a number of permanent magnets were arranged. An air line was attached to the orifice and a simple hanging fixture was incorporated in the disc for the attachment of the negator spring assembly.

The magnetic air pad was placed in contact with an overhead steel plate and compressed air was forced through the central orifice. This caused the air pad to float at some small distance from the ferro-magnetic surface, thus giving the device its low friction characteristic.

A prototype device (see Figure 4) four inches in diameter fitted with an Alnico magnet and operating at 75 - 80 psi was found to support a load of 55 pounds demonstrating the feasibility of the method.

Figure 5 shows a schematic of the magnetic air pad and gives the basic physical parameters which governed its performance. For static equilibrium in the vertical direction the following relationship was established.

$$\Sigma F_Z = - F_L + F_M + 2\pi \int_0^R (P_a - P_r)\, r dr = 0$$

or $$F_L = F_M + 2\pi \int_0^R (P_a - P_r)\, r dr$$

$$F_L = F_M + F_{air}$$

It is known that the magnetic force F_M is simply a function of the distance h. For any particular permanent magnet, this function can be determined by a simple experiment.

The pressure acting on the upper side of the disc P_r was assumed to be a function of the radial location r, the height of the disc from the surface h, the stagnation pressure P_o and the orifice diameter. Figure 6 shows the relationship between P_r, r and h for fixed values of P_o and the orifice diameter. This data was obtained with the experimental test arrangement shown in Figure 7.

Theoretical works by Mori (Ref. 2) and Robinson (Ref. 3) explain the shape of the experimentally observed pressure profiles. These analyses predict a supersonic flow issuing from the orifice followed by a shock wave in the bearing clearance space. The analyses yield good qualitative agreement with the experimental results shown in Figure 6.

The relationship between F_{air}, the force due to the air pressure, and h, the air gap, can be determined directly from experiment or can be derived from the pressure profile data. Figure 8 shows the typical form of the relationship. The curve is divided into four regions – A, B, C and D. In region A the force is negative which means that the net force due to air pressure is in the negative z direction. In regions B and C the net force due to the air pressure is positive. In other words, an air pad without magnets is capable of supporting a hanging load in both regions.

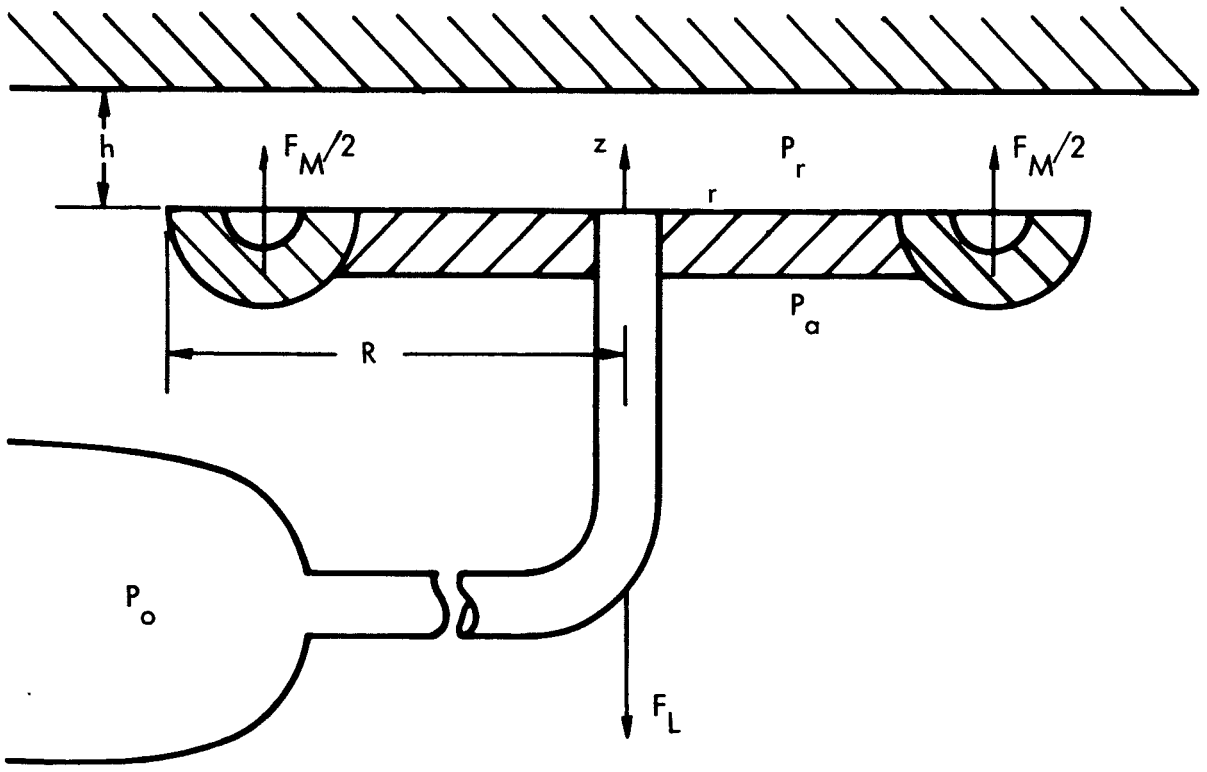

r = Radius

h = Air Gap

R = Radius of the disc

P_o = Stagnation pressure

P_a = Ambient pressure

P_r = Pressure acting on the upper surface of the disc

F_M = Magnetic force

F_L = Load

F_{AIR} = Force due to air pressure

Figure 5. - Schematic of magnetic air pad

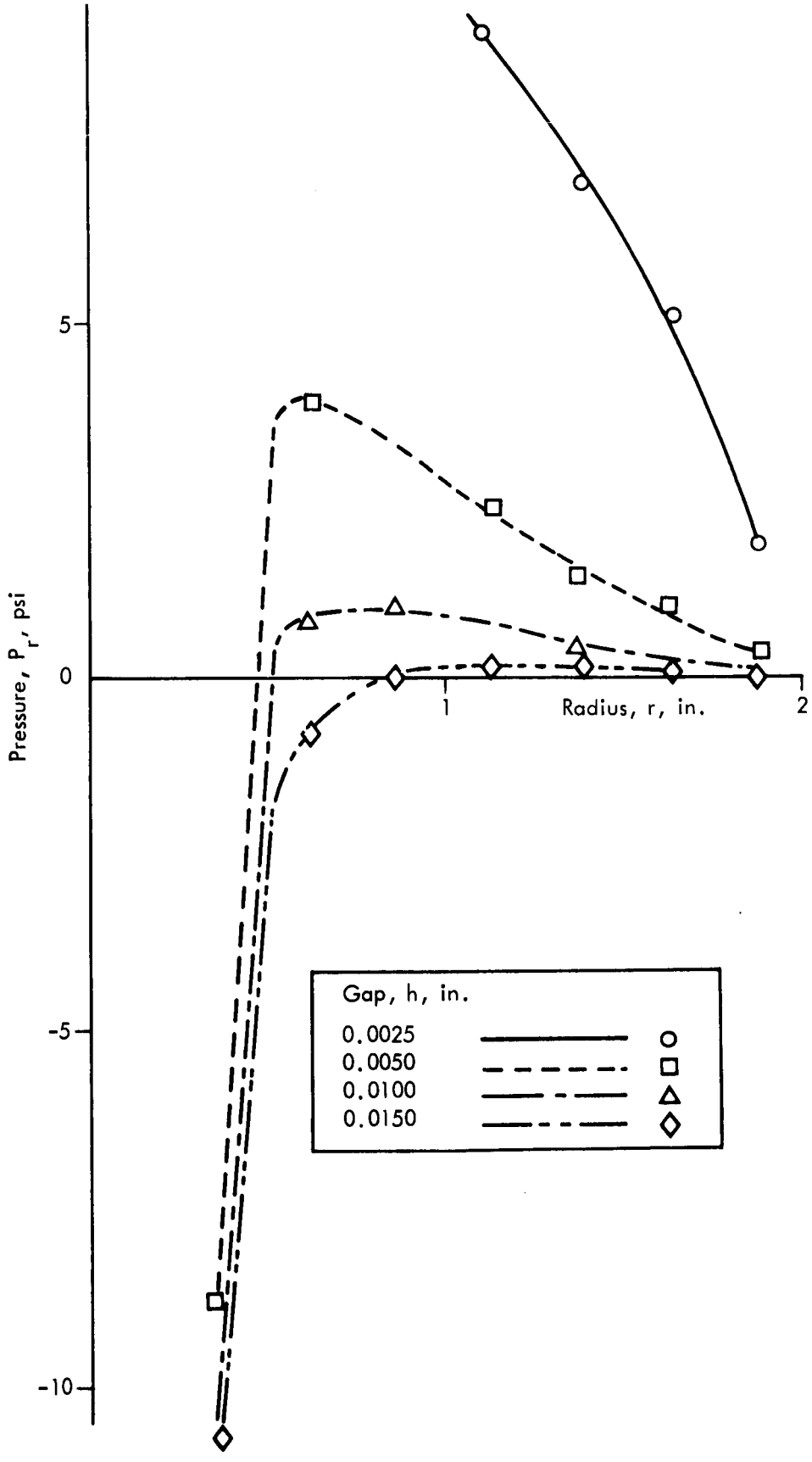

Figure 6. - Pressure profiles for various air gaps under 70 psi supply pressure

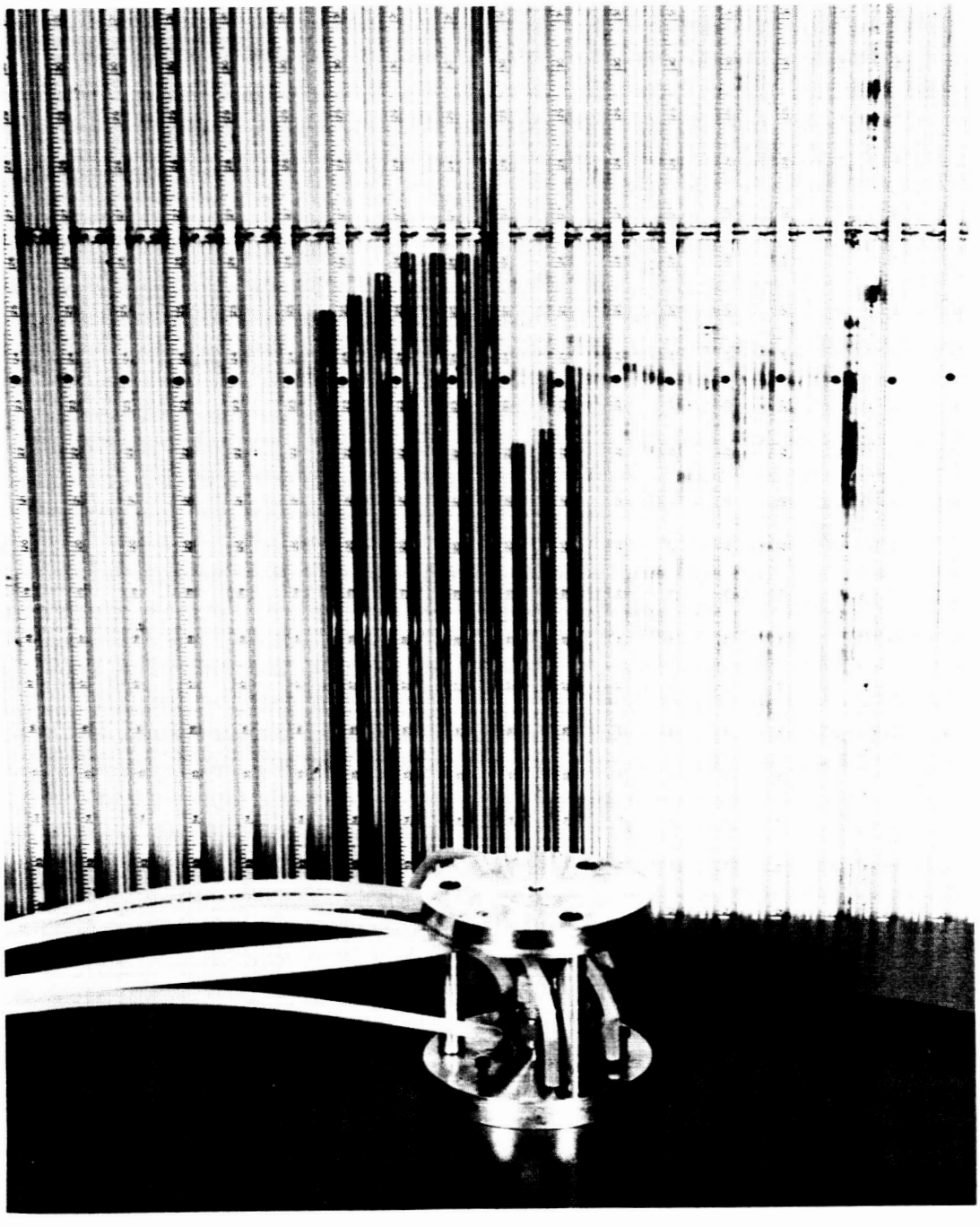

Figure 7. - Experimental test arrangement

The slope of the curve in regions A and B was positive. This meant that the air pad operating in either one of these regions was stable.* For instance, if an operating point in region B was chosen, the air pad was in equilibrium at that point. If for some reason the air pad was perturbed such that h increased slightly, the force F_{air} increased, thus driving the air pad back to its original position. The same general argument can be used to show that region A was stable.

*Although these comments refer to static stability no problems have been encountered with dynamic instability and the chosen design has proved to have very good dynamic characteristics when compared to other configurations. See Gross, Ref. 4.

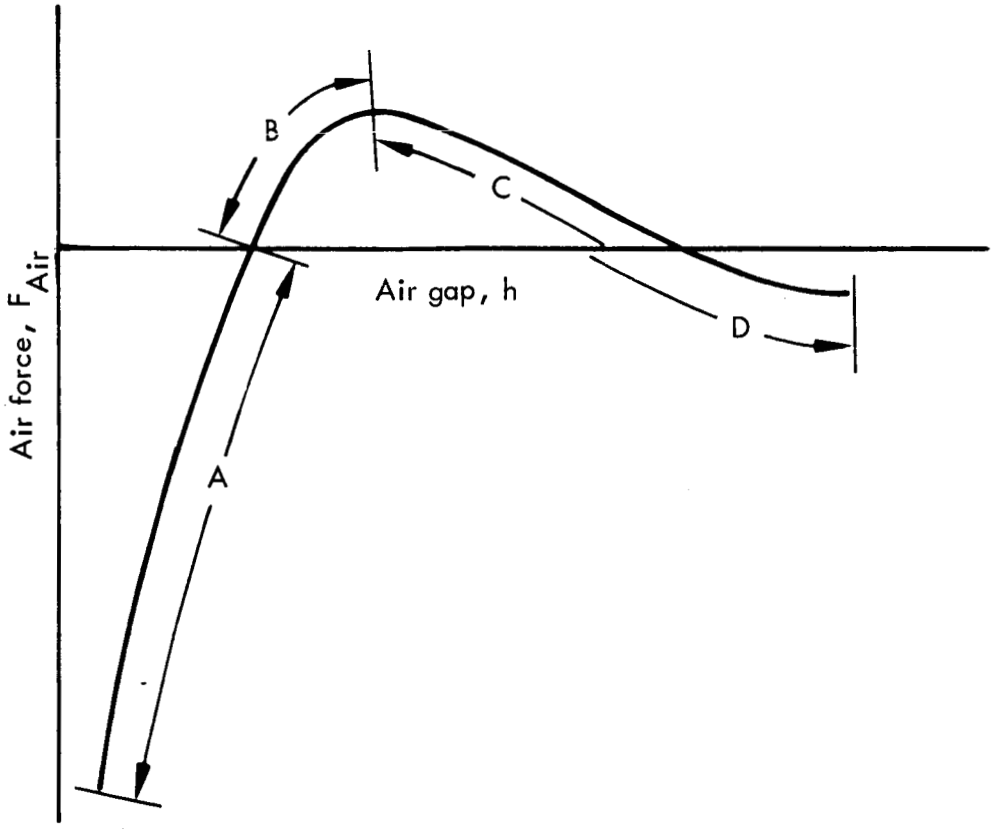

Figure 8. - Relationship of air force vs. air gap

In region C and a portion of region D the slope of the F_{air} versus h curve was negative. Here, if the air pad was perturbed slightly such that h increased there was no driving force toward the original equilibrium position. These regions of negative slope were therefore unstable.

The general shape of the magnetic force F_M versus air gap curve is shown in Figure 9. It is worthwhile to note that the slope of this curve was negative. This meant that a magnet supporting a hanging load at some distance from a ferro-magnetic surface is by itself unstable.

Recalling the derived equation for the static load which the magnetic air pas was capable of supporting, it is seen that the F_L versus h curve was simply the sum of the F_{air} versus h curve and the F_M versus h curve.

Figure 10 shows this summation. For stable operation, the air pad must operate on the positive slope portion, ABC, of the F_L curve. For fail-safe operation (in case of air supply failure), however, the pad must operate with an air gap less than h_b as defined by the intersection of the F_{air} curve with the zero load point. In other words, if h is less than h_b, the effect of cutting off the air supply will be to cause the disc (plus negator spring assembly) to adhere to the steel ceiling by virtue of the magnetic attraction which is then greater than the load.

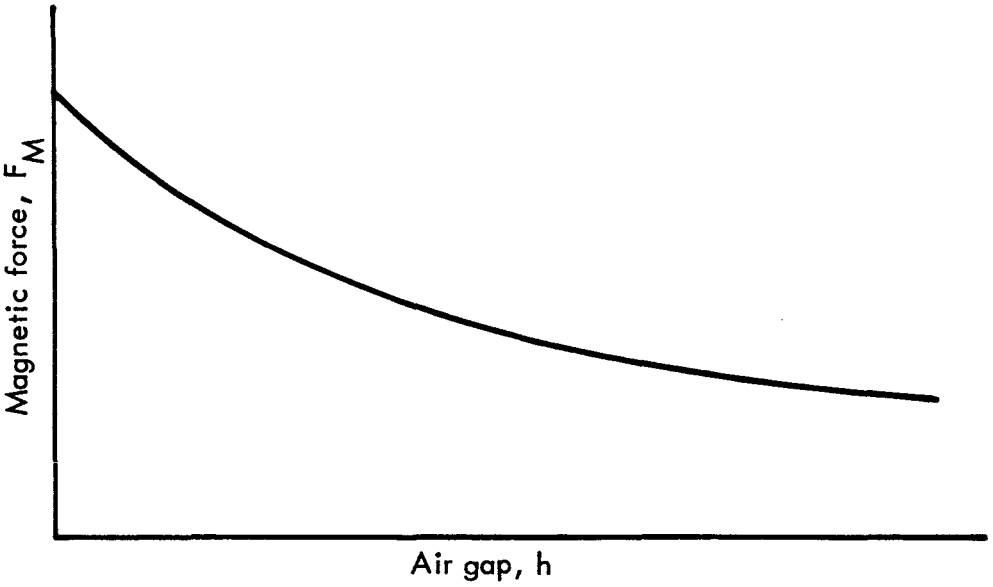

Figure 9. - Relationship of magnetic force vs. air gap

Although the experimental and theoretical investigation of the physical behavior of the magnetic air pad is not yet completed, sufficient data is now available to permit the design of a system to support the weight of a fully grown man.

Some experiments have been conducted on an annular orifice type pad and a central recess type pad but both designs proved to be inferior to the central orifice design employed in this application.

Safety Devices

Since the magnetic air pad is not rigidly attached to the ceiling some form of safety device will be needed in order to protect the user in the event of a break-away. This aspect of the problem has not been given much attention so far but is unlikely to produce any major difficulties.

One feasible method is to suspend a catching grid immediately below the negator spring assembly. The grid could be supported by wires attached to the corners of the room at roof level or thereabouts so that when a break-away occurs the equipment is held in suspension well above floor level.

The suspension wire system will need to incorporate spring loaded coiler-decoiler devices in order to take up and give out slack as the test subject moves within the confines of the test area.

As soon as a break-away occurs, the coilers must lock -- this can be achieved by fitting solenoid operated brakes to the coiler units. The sensing element which activates the brakes could be a microswitch attached to the magnetic air pad and making sliding contact with the ceiling in which case the switch is closed and the brake shoes are held in the open position. Once a break-away occurs, the microswitch opens and the power supply to the solenoids is shut off thus causing the brakes to lock on.

The possibility of accidental operation of the microswitch by local variations in ceiling height can be obviated by suitable choice of microswitch travel -- say, one-half inch. The system is basically "fail-safe" in operation since the brakes lock on whenever the circuit opens irrespective of the cause.

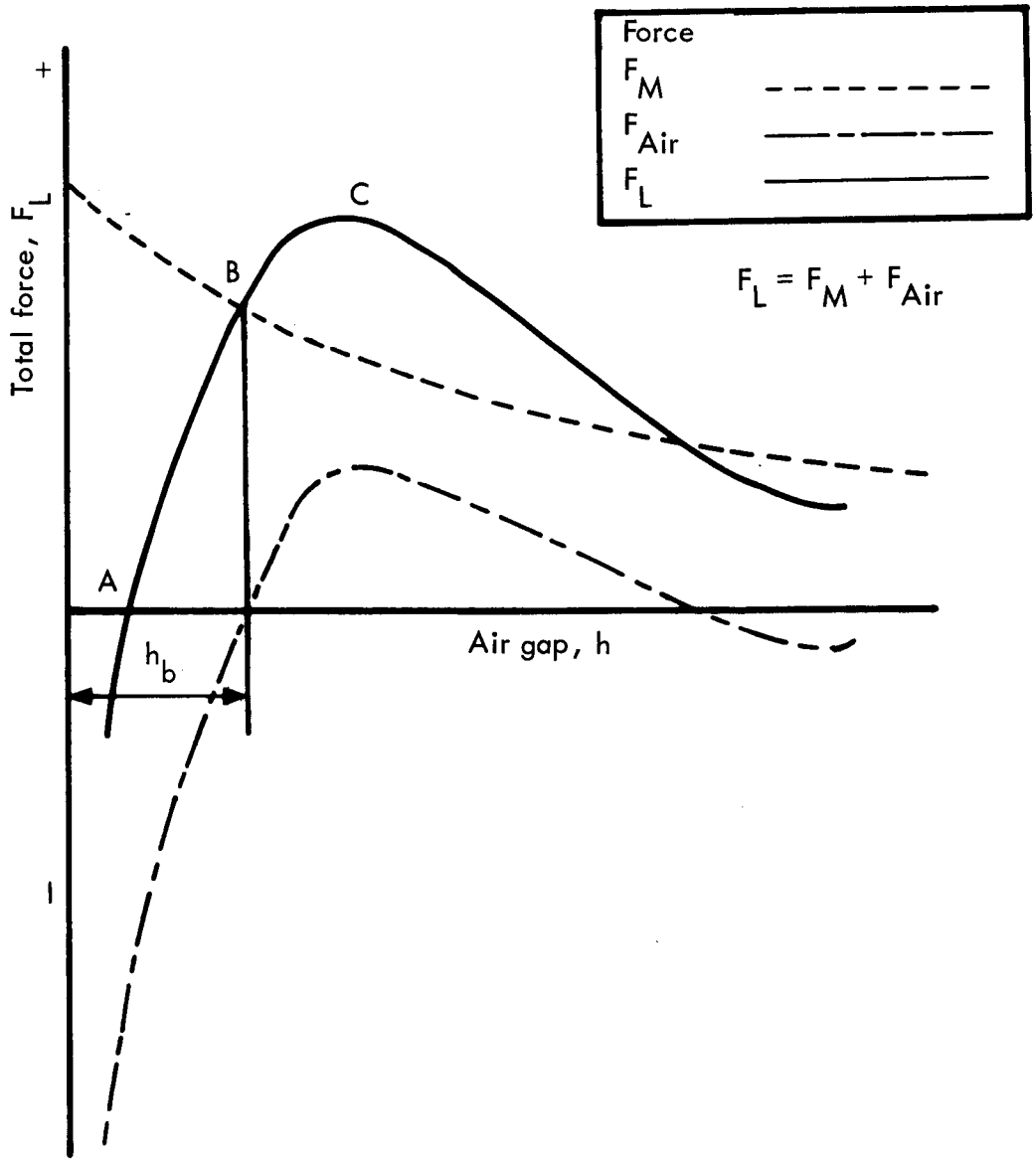

Figure 10. - Graphical summation of magnetic and air forces

SECTION 3

DESIGN AND DEVELOPMENT OF BODY HARNESS AND LIMB SUPPORT MECHANISMS

The body support system that has been designed applies 5/6 g negating forces to the body and limbs in a way which provides the most natural feel of 1/6 g simulation, along with the maximum possible freedom of body and limb movement and the minimum amount of interference with body and limb movement by supporting cables. In testing, it was found that this system has just under 4-1/2 degrees of freedom.

The torso support system, which was prototyped, consisted of a rigid saddle structure which the subject straddled plus straps to and over the shoulders. His torso weight was distributed through four bone points on his pelvis; the anterior superior iliac spine below his waist and the ischial tuberosities below his torso. See Figure 11. The 5/6 g negation forces were taken through points at about the collar bone on the shoulder straps and at points on either side of the hips of the saddle structure. The harness was found to be very comfortable during all tests. Padding was provided at the shoulders and at the points of contact below the waist.

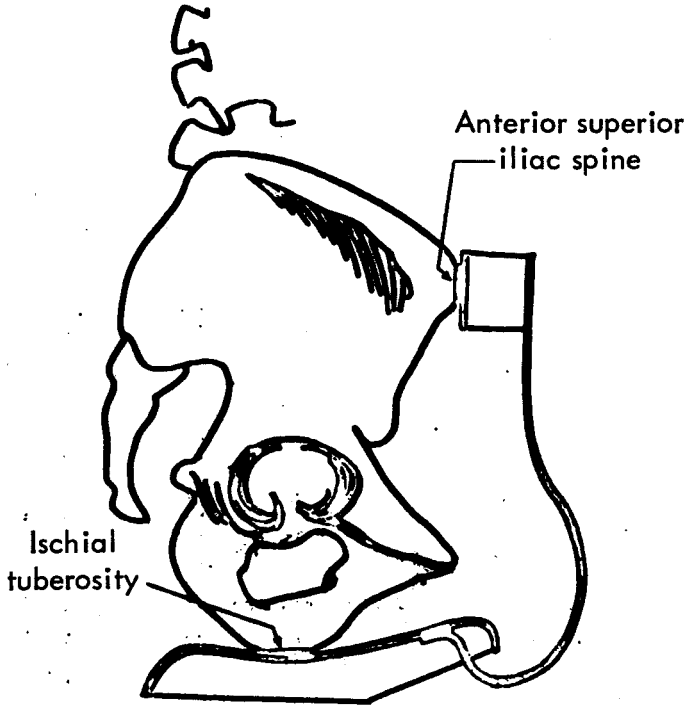

Figure 11. - Saddle structure

The inclined plane simulator was used as a control to compare the feel of 1/6 g simulation, freedom of body and limb movement and support interference.

The lower leg support consisted of a brace running the length of the lower leg with an arm prejecting under the instep of the foot. This brace was fastened to the leg with straps above the calf and at the arch of the foot at the instep. The suspension cable attachment point was located below the pivot point of the knee.

Support for the entire arm was provided by a brace strapped at a point below the elbow pivot point.

The exact positions of the leg and arm suspension cable attachment points was chosen so that the weight of the upper limb was distributed equally between the body and lower limb supports.

The negation load of the head was taken through a helmet which was fitted with a gimbal to allow forward, backward and side to side movement. The support cable allowed for pivoting.

All support cables led directly to the negating units. Exceptions to this direct arrangement occurred in the leg support cables which went through guides attached to the body harness. These guides led the leg support cables to the back of the subject and out of the way of his arms for all controlled maneuvering positions. This resulted in some diminution of negation forces to the legs when the cable from the harness guide to the leg was not vertical but this was considered to be unimportant relative to the principal function of the guides.

The present equipment was designed to give the body a pitch movement around the X axis of 110° and a roll movement about the Y axis of 15° in the vertical and prone positions.

Experiments were conducted on the body and limb support system described above with the various segments of the body being counterbalanced by weights approximately 5/6 of the weight of the segment. The supporting cables passed through ball bearing pulleys which were fastened to an overhead support 30 feet from the floor and then through another series of pulleys 12 feet from the first so that the hanging counterweights would not interfere with the subject. The set of pulleys directly above the subject was designed to pivot through 180° to enable the subject to move freely about the Z axis. The overall arrangement is sketched in Figure 12.

Experiments on this vertical prototype mockup with casual subjects are shown in Figures 13 through 17. They indicated that the simulation of a 1/6 g situation was fully as good as on the inclined plane simulator. The vertical orientation of the subject heightened the feeling of reduced gravity because of orientation to normal surrounding objects. Gross-motor activities such as jumping, simulated walking, running or leaping had the same feel as on the inclined plane simulator. Falling over was almost as good as on the inclined plane. Support cable interference occurred when the subject rotated backwards around his X axis to simulate a rearwards fall. If the subject rotated backwards more than 15° from the vertical position, the leg and lower torso support cables tended to pass around his arms to a position in front of him. The 15° rearward rotation, however, was considered sufficient to indicate to the subject that he had lost his balance.

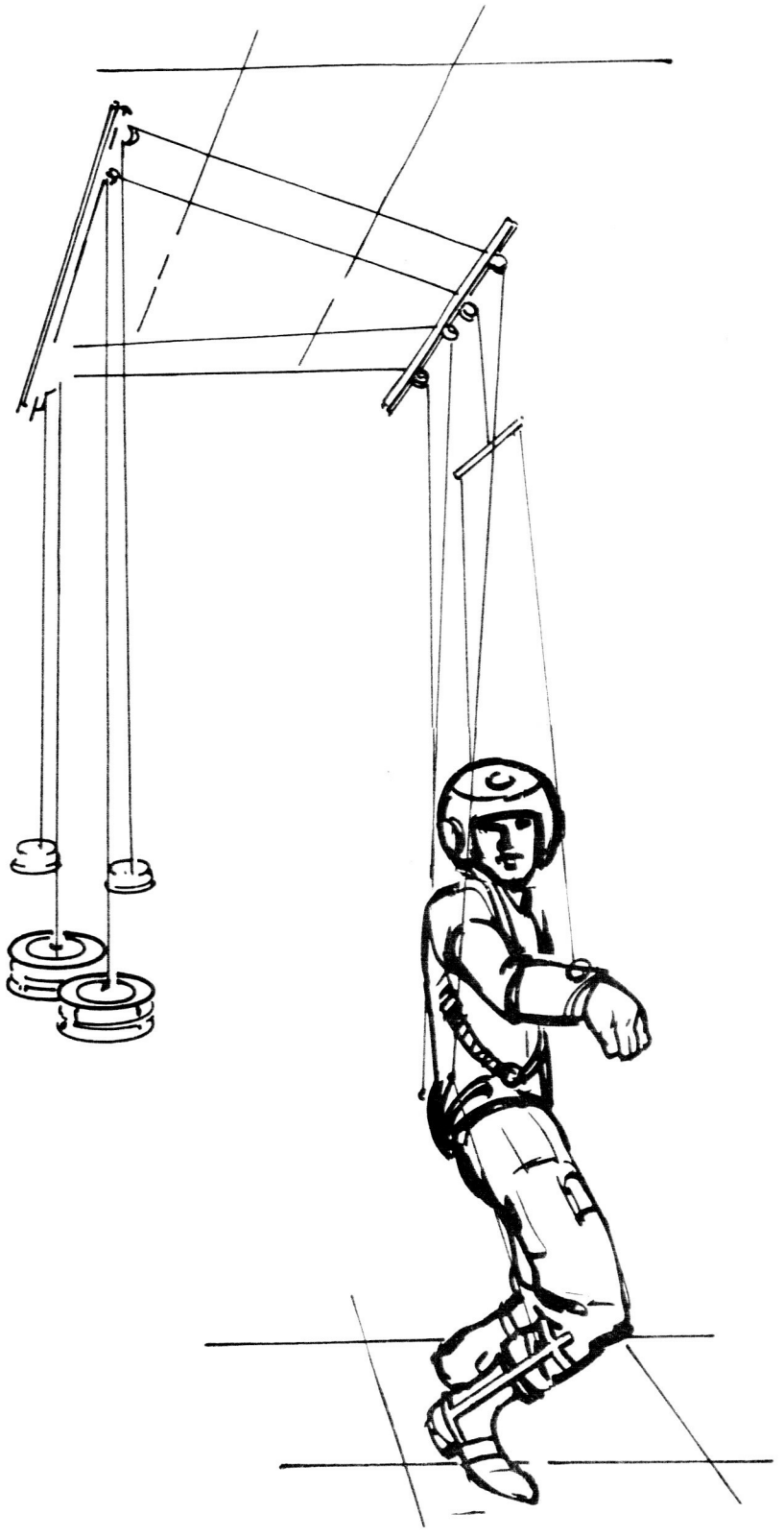

Figure 12. - Counter balance suspension

Figure 13. - Subject front view

Figure 14. - Subject side view

Figure 15. - Subject jumping

Figure 16. - Subject crawling

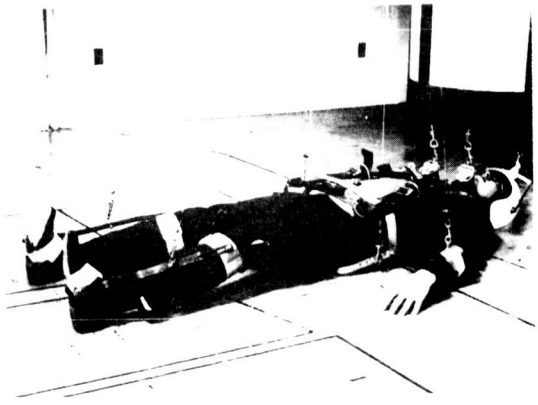

Figure 17. - Subject on back

Support cable interference also occurred when the subject tried to make a complete crossover of his arms in front of his body. It is not known at present whether this interference can be easily overcome but if this semigross motor activity had to be executed, then the arm support cables could be disconnected.

It was generally felt that the inertia of the counterweights caused movements to be somewhat slower than on the inclined plane, but this effect should be largely eliminated when negator springs are employed.

Figures 13 through 17 are a series of photographs designed to illustrate the harness design and the freedom of movement available to the test subject.

CONCLUSIONS

The work which has been carried out on the inclined plane simulator showed that this type of system could be further refined to give the subject additional freedom of movement and an attempt has been made to show how this could be done.

The most important part of the report was devoted to the vertical suspension type simulator. This type of simulator will permit the test subject to perform maneuvers which are difficult or impossible to perform on the inclined plane. Although much work still remains to be done, the experience now available clearly shows that the method is practical.

The system has the advantages that the test subject is supported in the normal upright position and is able to move anywhere within the confines of the test area. It also provides him with sufficient freedom to perform most normal activities such as walking, running, changing direction, etc.

The present harness has been evolved after prolonged testing and experimentation and now provides a high degree of comfort to the test subject.

The next logical step in the overall development process is the design and construction of a full size prototype system; sufficient basic design data has now been accumulated to enable this step to be taken.

RECOMMENDATIONS

The following recommendations by tasks are made to indicate the importance of continuing this work in the interest of improving lunar gravity simulation techniques:

Task 1: The work on the magnetic air pad systems should be completed by experimentation and analyses for recommended and optimal suspension units. These recommendations shall include the design, radius, the magnet and air bearing flow rates.

Task 2: Should be performed to finalize the work on the negator spring system suspended from the magnetic air pad. This should include information for recommending the

- selection of springs
- attachment of springs
- dynamics of spring including the fatigue life and replacement schedule

Task 3: Design and development of a harness and limb support mechanism for vertical subject suspension. This harness should be made adjustable to accommodate a range of subjects in the shirt sleeve and pressure suited condition.

Task 4: Production of a vertical suspension prototype for the simulation of lunar gravity. This prototype should employ the recommended magnetic air pad developed under Task 1, the recommended negator spring system from Task 2 and the harness recommended in Task 3. A safety mechanism should be installed and tested frequently/or prior to each test run. This safety mechanism must be designed to prevent at all times the magnetic air pads and remaining suspension gear from falling onto the subject or the floor below.

Task 5: Tests should be performed with the prototype developed under Task 4. Two or more subjects should be used to determine

- the physical space available for lunar gravity stimulation experiments
- the types of experiments that can be conducted with the vertical suspension device
- the dynamic response limitations, distortions or any other limitations observed during the tests
- the effects of partially negated suspension versus total suspension

REFERENCES

1. Hewes, D.E., and Spady, A.A., Evaluation of a Gravity Simulation Technique for Studies of Man's Self-Locomotion in Lunar Environment, NASA Technical Note, TND-2176, 1964.

2. Mori, Harvo: A theoretical investigation of pressure depression in externally pressurized gas-lubricated circular thrust bearings. J. Basic Eng., Trans. ASME, 83, 1961. pp. 201-208.

3. Robinson, G.M.: A special analytical study of air lubricated bearings for jet aircraft engines. Final Technical Report F-A1914, contract no. NAW 6473. National Advisory Committee for Aeronautics, Feb. 15, 1957.

4. Gross, W.A.: Gas Film Lubrication, Wiley, N.Y., 1962.

BIBLIOGRAPHY

Boeker, C. F.; Fuller, D. D.; and Kayan, C. F.: Gas-lubricated Bearings, a critical survey. AF 33 (616) - 5054, Project 3066, Task 70532, Wright Air Development Center, July 1958.

Grinnell, S. K.; Flow of a compressible fluid in a thin passage. Trans. ASME, May 1956, pp. 765-771.

Kuhnegger, W.: N. S. L. Internal Report, N. S. L 64 - 151, pg. 19.

Licht, L. and Elrod, H. G.: An analytical and experimental study of the stability of externally pressurized gas lubricated thrust bearings. Contract Nonr. 2342 (00) Task NP 061-113. Office of Naval Research, February 1961.

Licht, L.; Fuller, D. D. and Sternlicht, B.: Self-excited vibrations of an air-lubricated thrust bearing. Trans. ASME, Feb. 1958, pp. 411-414.

Licht, L.; Axial relative motion of a circular step bearing. Trans. ASME, June 1959, pp. 109-117.

Stevenson, C. and Licht, L.; Experimental determination of stability boundaries for an externally-pressurized gas-lubricated thrust bearing. Contract Nonr. - 2342 (00). Task N R 061-113, Franklin Institute, Feb. 1962.

Votta, F. A.: The theory and design of long-deflection, constant-force spring elements. Trans. ASME, May 1952, pp. 439-450.

APPENDIX A

ANALYSIS OF SYSTEM DYNAMICS

Introduction

This appendix contains an abbreviated version of an analysis of the dynamic behavior of a vertical suspension type simulator The system to be analyzed is shown in Figure A1. and is a simplified version of the real system shown in Figure 3.

The system components consist of one magnetic air pad, a back-to-back negator spring assembly and the subject mass. The subject mass will be considered to be inanimate. The negator spring assembly housing is attached to the air pad by a ball joint. If the system is confined to move in a plane perpendicular to the ceiling, its position can be defined by three generalized coordinates; namely, the position of the air pad center of gravity, the angle between the extended negator springs and the vertical, and the distance from the ball joint to the subject mass. An important assumption must be made, however, before these three coordinates can correctly determine the position of the system. This is that the extended portion of the negator spring does not bend in the plane of motion. This is probably a valid assumption for the orientation of the negator springs shown in Figure A1.* If, however, the negator spring assembly were rotated through 90 degrees, the width of the negator springs would be perpendicular to the plane of motion. Due to the very low rigidity of the negator springs in this direction, the assumption would no longer apply and the three coordinates would not suffice in locating the system.

The following are the assumptions which will be made in the derivation of the dynamic equations:

1. The extended portion of the negator spring is rigid and inextensible.
2. The air pad moves with negligible friction.
3. The up-and-down dynamics of the air pad are so small that they can be neglected.
4. The ball joint has negligible friction.
5. The air drag on the system is negligible.
6. The motion of the system is planar.
7. The negator spring system has a constant force for any elongation.

The parameters used in the analysis are defined as follows:

x_p Location of the center of gravity of the air pad.

* Note that the width of the negator spring is parallel to the plane of motion.

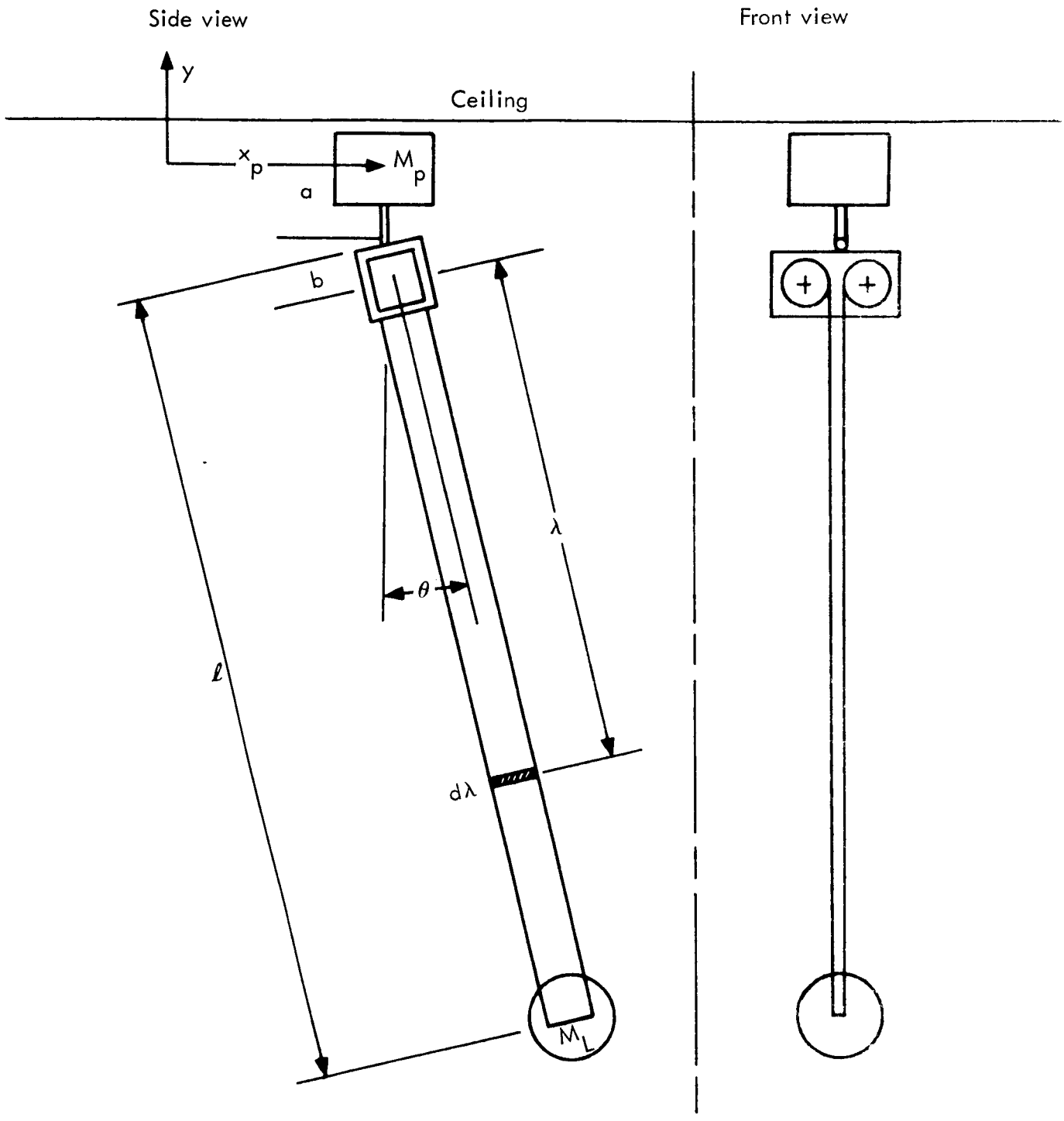

Figure A1. - Mathematical model of lunar gravity simulator

θ Angle that the extended portion of the negator spring makes with the vertical.

ℓ The distance from the ball joint to the center of gravity of the subject mass.

a The distance from the center of gravity of the air pad to the ball joint.

b The distance from the ball joint to the center of gravity of the negator spring spools and housing.

r_s Radius of a negator spring spool.

R Radius of the coiled portion of negator spring.

W Width of the negator spring.

t Thickness of the negator spring.

L Total length of a negator spring.

D_{cg} The center of gravity of the system of masses suspended from the ball joint measured from that point.

λ A distance parallel to any point on the extended portion of the negator spring.

x Horizontal distance from a reference point.

y Vertical distance from a reference point.

M_L Mass of the subject.

M_p Mass of the air pad.

M_h Mass of the negator spring housing.

M_s Mass of a negator spring spool containing bearings.

M_e Mass of the extended portion of one negator spring.

M_c Mass of the coiled portion of one negator spring.

ρ The density of the negator spring material.

I_{so} Moment of inertia of one spool about the ball joint.

I_{co} Moment of inertia of the coiled portion of one negator spring about the ball joint.

I_{ho} Moment of inertia of the negator spring housing about the ball joint.

$I_{s\alpha}$ Moment of inertia of one spool about its axis of rotation.

I_c Moment of inertia of the coiled portion of one negator spring about the axis of rotation.

F The force output of both negator springs.

T The kinetic energy of the system.

Q A generalized force.

D_m Damping coefficient.

τ A torque.

τ_f Coulamb bearing friction torque.

Kinetic Energy of the Extended Portions of Negator Springs

With reference to Figure A1, the position of any element of mass along the extended portion of the negator spring can be written

$$x_\lambda = x_p + \lambda \sin \theta \tag{A1}$$

$$y_\lambda = -a - \lambda \cos \theta \tag{A2}$$

The component velocities of any element of mass can be found by differentiating the above positions with respect to time.

$$\dot{x}_\lambda = \dot{x}_p + \dot{\lambda} \sin \theta + \lambda \dot{\theta} \cos \theta \tag{A3}$$

$$\dot{y}_\lambda = -\dot{\lambda} \cos \theta + \lambda \dot{\theta} \sin \theta \tag{A4}$$

The kinetic energy of the extended portions of both negator springs can be written as

$$T_e = \rho wt \int_b^\ell \left(\dot{x}_\lambda^2 + \dot{y}_\lambda^2\right) d\lambda \tag{A5}$$

Upon substitution of the squares of the component velocities into the above expression, the kinetic energy can be written

$$T_e = \rho wt \int_b^\ell (\dot{x}_p^2 + \dot{\lambda}^2 + \lambda^2 \dot{\theta}^2 + 2\dot{x}_p \lambda \sin \theta + 2\dot{x}_p \lambda \dot{\theta} \cos\theta)\ d\lambda \tag{A6}$$

It should be noted that $\dot{\lambda}$ is a constant over the integration which takes place at any instant of time. In addition, $\dot{\lambda}$ must be equal to $\dot{\ell}$ due to physical constraint. Upon completing the integration and making the above-mentioned substitution, the kinetic energy of the extended portion of both negator springs can be expressed as follows:

$$T_e = \rho wt \{[\dot{x}_p^2 + \dot{\ell}^2 + 2\dot{x}_p \dot{\ell} \sin \theta]\,[\ell - b] + \frac{\dot{\theta}^2}{3}\,[\ell^3 - b^3] + \dot{x}_p \dot{\theta} \cos\,\theta[\ell^2 - b^2]\} \tag{A7}$$

Kinetic Energy of the Subject Mass

For the sake of simplicity, the mass M_L will be assumed concentrated at a point. The coordinates of this point are

$$x_L = x_p + \ell \sin\theta \tag{A8}$$

$$\lambda_L = -a - \ell \cos\theta \tag{A9}$$

The velocities of this point are found by differentiating the above coordinates with respect to time.

$$\dot{x}_L = \dot{x}_p + \dot{\ell}\sin\theta + \ell\dot{\theta}\cos\theta \tag{A10}$$

$$\dot{y}_L = -\dot{\ell}\cos\theta + \ell\dot{\theta}\sin\theta \tag{A11}$$

The kinetic energy of the mass can be written

$$T_L = \frac{1}{2} M_L (\dot{x}_L^2 + \dot{y}_L^2) \tag{A12}$$

Upon making the appropriate substitutions, the kinetic energy of the subject mass is

$$T_L = \frac{1}{2} M_L (\dot{x}_p^2 + \dot{\ell}^2 + \ell^2\dot{\theta}^2 + 2\dot{x}_p\dot{\ell}\sin\theta + 2\dot{x}_p\ell\dot{\theta}\cos\theta) \tag{A13}$$

Kinetic Energy of the Negator Spring Housing

The coordinates of the center of gravity of the negator spring housing are

$$x_h = x_p + b\sin\theta \tag{A14}$$

$$y_h = -a - b\cos\theta \tag{A15}$$

The velocities are

$$\dot{x}_h = \dot{x}_p + b\dot{\theta}\cos\theta \tag{A16}$$

$$\dot{y}_h = b\dot{\theta}\sin\theta \tag{A17}$$

The kinetic energy of the housing can then be written as

$$T_h = \frac{1}{2} M_h (\dot{x}_p^2 + b^2\dot{\theta}^2 + 2\dot{x}_p b\dot{\theta}\cos\theta) + \frac{1}{2} I_{hcg}\dot{\theta}^2 \tag{A18}$$

Using the parallel axis theorem, the moment of inertia of the housing about the ball joint is

$$I_{h\theta} = I_{hcg} + M_h b^2 \tag{A19}$$

Substituting this equation into the expression for kinetic energy yields the following:

$$T_h = \frac{1}{2} M_h (\dot{x}_p^2 + 2\dot{x}_p b \dot{\theta} \cos\theta) + \frac{1}{2} I_h \theta \dot{\theta}^2 \tag{A20}$$

Kinetic Energy of Both Negator Spring Spools

The coordinates of the center of gravity of the two-spool combination are

$$x_s = x_p + b \sin\theta \tag{A21}$$

$$y_s = -a - b \cos\theta \tag{A22}$$

The corresponding velocities of this center of mass are

$$\dot{x}_s = \dot{x}_p + b \dot{\theta} \cos\theta \tag{A23}$$

$$\dot{y}_s = b \dot{\theta} \sin\theta \tag{A24}$$

The spools rotate with an angular velocity $\dot{\alpha}$. This angular velocity is a function of both $\dot{\ell}$ and ℓ, and can be expressed as

$$\dot{\alpha} = \frac{\dot{\ell}}{R} \qquad R = \sqrt{\frac{t}{\pi}(L + b - \ell) + r_s^2} \tag{A25}$$

where R is the variable radius of a coil. The expression for R is derived in the next section.

Solving for the kinetic energy due to translation of the center of mass plus that due to rotation about the center of mass gives

$$T_s = M_s [x_p^2 + 2x_p b \theta \cos\theta] + I_{so}\theta^2 + I_s \alpha \frac{\dot{\ell}^2}{[\frac{t}{\pi}(L + b - \ell) + r_s^2]} \tag{A26}$$

Kinetic Energy of the Coiled Portions of Both Negator Springs

The coordinates of the center of mass of the coil are

$$x_c = x_p + b \sin\theta \tag{A27}$$

$$y_c = -a - b \cos\theta \tag{A28}$$

It should be noted that these coordinates are not a function of the variable ℓ.

The velocities of the center of mass are

$$\dot{x}_c = \dot{x}_p + b \dot{\theta} \cos\theta \tag{A29}$$

$$\dot{y}_c = b\dot{\theta} \sin\theta \tag{A30}$$

The kinetic energy of the coils can be expressed as

$$T_c = M_c (\dot{x}_p + 2\dot{x}_p b \dot{\theta}\cos\theta) + I_{c\theta}\dot{\theta}^2 + I_{\alpha c}\frac{\dot{\ell}^2}{R^2} \tag{A31}$$

The parameters M_c, $I_{c\theta}$ and $I_{\alpha c}$ are functions of the distance ℓ.

It can be easily seen that the mass of one coil is

$$M_c = \rho wt (L + b - \ell) \tag{A32}$$

The radius of the coil can be found from the evaluation of the following integral.

$$\int_{r_s}^{R} rdr = \int_{o}^{C} \frac{t}{2\pi} ds \tag{A33}$$

Where C is the length of the coiled negator spring and ds is an element of arc length.

$$C = L + b - \ell \tag{A34}$$

Upon evaluation of the above integral, R is found.

$$R = \sqrt{\frac{t}{\pi}(L + b - \ell) + r_s^2} \tag{A35}$$

The moment of inertia of one coil about its cylindrical axis is

$$I_{\alpha c} = \frac{\pi}{2}\rho w\left[R^4 - r_s^4\right] \tag{A36}$$

The moment of inertial of a coil about an axis perpendicular to the axis of symmetry through the ball joint is

$$I_{\theta c} = m_c\left[\frac{(R^2 - r_s^2)}{4} + \frac{W^2}{12} + b^2\right] \tag{A37}$$

Making the appropriate substitutions, the kinetic energy of both coils is found.

$$T_c = \rho wt (L + b - \ell)(\dot{x}_p^2 + 2\dot{x}_p b \dot{\theta}\cos\theta)$$

$$+\rho wt\,(L+b-\ell)\left[\frac{t}{4\pi}\,(L+b-\ell)+\frac{W^2}{12}+b^2\right]\dot{\theta}^2$$

$$+\frac{\ell}{2}\rho wt\,(L+b-\ell)\frac{\left[\frac{t}{\pi}(L+b-\ell)+2r_s^{\,2}\right]\dot{\ell}^2}{\left[\frac{t}{\pi}(L+b-\ell)+r_s^{\,2}\right]} \qquad \text{(A38)}$$

Kinetic Energy of the Air Pad

The kinetic energy of the air pad can be simply expressed by

$$T_p=\frac{1}{2}m_p\dot{x}_p^{\,2} \qquad \text{(A39)}$$

Kinetic Energy of the System

The kinetic energy of the system is the summation of the kinetic energies of the component masses.

$$T=T_e+T_\ell+T_h+T_s+T_c+T_p \qquad \text{(A40)}$$

Generalized Forces

Because of the negligible air drag assumption, the generalized force due to a variation in x_b is

$$Q_{x_b}=0$$

Using the assumptions of negligible air drag and friction in the ball joint, the generalized force due to the variation of θ is

$$Q_\theta=-g\,(M_L+M_h+2M_g+2M_c+2M_e)\,D_{cg}\sin\theta \qquad \text{(A41)}$$

Where D_{cg} is the center of mass of the system suspended below the ball joint.

$$D_{cg}=\frac{b\,(2M_s+M_h)+\ell M_L+2\rho wtbL+\rho wt(\ell-b)^2}{M_L+M_h+2M_s+2M_c+2M_e} \qquad \text{(A42)}$$

Q_θ can now be expressed as

$$Q_\theta=-g\,[\,b\,(2M_s+M_L)+\ell M_L+2\rho wtbL+\rho wt(\ell-b)^2\,]\sin\theta \qquad \text{(A43)}$$

In calculating the generalized force due to a variation in ℓ, the frictional torque in the bearings of one negator spring spool is assumed to be of the form

$$\tau = -(D_m \dot{\alpha} + \frac{\dot{\alpha}}{|\dot{\alpha}|} \tau_f) \tag{A44}$$

The frictional torque contains a viscous friction term and a coulomb friction term. It will be assumed that these are independent of the load applied to the bearing because the variation in the bearing load should be small.

The frictional force due to this torque can be written $f = \frac{2\tau}{R}$ making the substitution $\dot{\alpha} = \frac{\dot{\ell}}{R}$.

The frictional force due to the bearings in the spools is

$$f = -2 (D_m \frac{\ell}{R^2} + \frac{\dot{\ell}}{|\dot{\ell}|} \frac{\tau_f}{R}). \tag{A45}$$

The generalized force due to a variation in ℓ is

$$Q_\ell = (2M_e + M_\ell)\, g \cos\theta - 2 (D_m \frac{\dot{\ell}}{R^2} + \frac{\dot{\ell}}{|\dot{\ell}|} \tau_f) - F \tag{A46}$$

Substituting the expressions for M_e and R into the above equation, Q_ℓ is found in terms of the generalized coordinates.

$$Q_\ell = [2 \rho wt (\ell - b) + M_L]\, g \cos\theta - \frac{2 [D_m \dot{\ell} + \frac{\dot{\ell}}{|\dot{\ell}|} \tau_f \sqrt{\frac{t}{\pi} (L + b - \ell) + r_s^2}]}{\frac{t}{\pi} (L + b - \ell) + r_s^2} - F \tag{A47}$$

Derivation of Dynamic Equations

Using the method of Lagrange, three dynamic equations will be derived. There will be one equation for each generalized coordinate or degree of freedom.

The first equation of motion for the system is

$$\frac{d}{dt} (\frac{\partial T}{\partial \dot{x}_p}) - \frac{\partial T}{\partial x_p} = Q_{xp}$$

$$\frac{\partial T}{\partial x} = 0 = Q_{xp}$$

Then $\frac{d}{dt} (\frac{\partial T}{\partial \dot{x}_p}) = 0$ (A48)

It is seen that the coordinate x_p can be ignored from the standpoint of the dynamics of the system. Furthermore, the above equation is immediately integrable and has the form

$$\frac{\partial T}{\partial \dot{x}_p} = \text{const.}$$

Since the quantity $\frac{\partial T}{\partial \dot{x}_p}$ is the momentum associated with the coordinate $\dot{x}_p$, the previous equation is a statement of conservation of momentum in the x_p direction.

Carrying out the required differentiation, this equation becomes

$$(M_p + M_h + 2M_s + 2\rho wtL + M_L)\,\dot{x}_p + (M_h + 2M_s + 2\rho wtL)\,b\,\dot{\theta}\cos\theta + M_L(\dot{\ell}\sin\theta + \ell\,\dot{\theta}\cos\theta) + \rho wt\,[(\ell - b)^2\,\dot{\theta}\cos\theta + 2(\ell - b)\,\dot{\ell}\sin\theta] = \text{const.} \tag{A49}$$

The second equation of motion for the system is

$$\frac{d}{dt}\left(\frac{\partial T}{\partial \dot{\theta}}\right) - \frac{\partial T}{\partial \theta} = Q_\theta \tag{A50}$$

Performing the required differentiations yields:

$$\ddot{\theta}\left[2/3\,\rho wt\left(\ell^3 - b^3\right) + M_L\ell^2 + I_{h\theta} + 2I_{s\theta} + \frac{\rho wt^2}{2\pi}\left(L + b - \ell\right)^2 + 2\rho wt\left(L + b - \ell\right)\left(\frac{w^2}{12} + b^2\right)\right] + \dot{\theta}\dot{\ell}\left[2\rho wt\ell^2 + 2\ell M_L - \frac{\rho wt}{\pi}\left(L + b - \ell\right) - 2\rho wt\left(\frac{w^2}{12} + b^2\right)\right] + \ddot{x}_p\left[\rho wt\left(\ell^2 + b^2\right)\cos\theta + M_L\ell\cos\theta + 2M_s b\cos\theta + 2\rho wt\left(L - \ell\right)b\cos\theta\right] + g\left[b\left(2M_s + M_L\right) + \ell M_L + 2\rho wtbL + \rho wt\left(\ell - b\right)^2\right]\sin\theta = 0 \tag{A51}$$

The third equation of motion for the system is

$$\frac{d}{dt}\left(\frac{\partial T}{\partial \dot{\ell}}\right) - \frac{\partial T}{\partial \ell} \quad Q_{\ell} \tag{A52}$$

The evaluation of this equation yields:

$$\ddot{\ell}\left\{2\rho wt\left(\ell - b\right) + M_L + 2I_{s\alpha} + \frac{\rho wt\left(L + b - \ell\right)\left[\frac{t}{\pi}\left(L + b - \ell\right) + 2r_s^2\right]}{\frac{t}{\pi}\left(L + b - \ell\right) + r_s^2}\right\}$$

$$+ \ddot{x}_p\left[2\rho wt \sin\left(\ell - b\right) + M_L \sin\theta\right]$$

$$+ \frac{t}{\pi}\dot{\ell}^2\left\{\frac{I_{s\alpha} + \frac{1}{2}\rho wt\left(L + b - \ell\right)\frac{t}{\pi}\left[\left(L + b - \ell\right) + 2r_s^2\right]}{\left[\frac{t}{\pi}\left(L + b - \ell\right) + r_s^2\right]^2}\right\}$$

$$+ \dot{\theta}^2\left\{\rho wt\left[\frac{t}{2\pi}\left(L + b - \ell\right) + \frac{w^2}{12} + b^2\right] - \rho wt\ell^2 - M_L\ell\right\}$$

$$= \left[2\rho wt\left(\ell - b\right) + M_L\right] g\cos\theta - F - \frac{2\left[D_m + \tau_f\frac{\dot{\ell}}{|\dot{\ell}|}\sqrt{\frac{t}{\pi}\left(L+b-\ell\right) + r_s^2}\right]}{\frac{t}{\pi}\left(L + b - \ell\right) + r_s^2} \tag{A53}$$

The three equations of motion are highly nonlinear and contain a great degree of dynamic coupling.

Linearization and Solution of Dynamic Equations

An attempt will be made to linearize and solve the previously derived equations of motion. Due to the highly nonlinear nature of the equations, it is obvious that any linear approximation will have an extremely limited application.

The First Equation of Motion

By making the following limitations and assumptions, the first equation of motion can be linearized:

θ - is limited to small angles

$\dot{\theta}$ - is small

$\dot{x}_p$ - is small

$\dot{\ell}$ - is small

The generalized coordinate ℓ can be written $\ell = \lambda + \epsilon$ where ϵ is small and λ is constant. Differentiating ℓ with respect to time $\dot{\ell} = \dot{\epsilon}$.

Substituting the above into the first equation of motion and using $\cos\theta \cong \ell$ and $\sin\theta \cong \theta$, the equation becomes:

$$(M_p + M_h + 2M_s + \rho wtL + M_L)\dot{x}_p + (M_h + 2M_s + 2\rho\, wtL)\, b\dot{\theta}\; M_L[\dot{\epsilon}\theta + (\lambda+\epsilon)\dot{\theta}] + \rho wt\; [(\lambda+\epsilon-b)^2\dot{\theta} + 2(\lambda+\epsilon-b)\dot{\epsilon}\;\theta] = \text{const.} \tag{A54}$$

Dropping terms of order two or more in the above-mentioned parameters, the first equation of motion is linearized.

$$A\dot{x}_p - B\dot{\theta} = \text{const.}$$

where A and B are the following constants:

$$A = M_p + M_h + 2M_s + 2\,\rho wtL + M_L \tag{A55}$$

$$B = (M_h + 2M_s + 2\,\rho wtL)\, b + M_L\,\lambda + \rho\, wt\,[\lambda - b]^2 \tag{A56}$$

The Second Equation of Motion

Assuming the following limitations:

θ - is limited to small angles

$\dot{\theta}$ - is small

ϵ - is small

and dropping terms of second order or more, the second quation of motion takes the form:

$$\ddot{\theta}C + \ddot{x}_p D + \theta E + \ddot{\theta}\epsilon F + \ddot{x}_p \epsilon G = 0 \tag{A57}$$

where C, D, E, F and G are constants.

If it is now required that the accelerations $\ddot{\theta}$ and $\ddot{x}_p$ are small and again dropping terms of second order, one obtains a linear differential equation.

$$\ddot{\theta}C + \ddot{x}_p D + \theta E = 0$$

where

$$C = 2/3\ wt\ (\lambda^3 - b^2) + M_L\ \lambda^2 + I_{ho} + 2I_s\theta + \frac{\rho wt^2}{2\pi}\ (L + b - \lambda) + 2\rho wt\ (L + b - \lambda)\left(\frac{w^2}{12} + b^2\right) \quad \text{(A58)}$$

$$D = \rho wt(\lambda^2 + b^2) + M_L\lambda + M_h b + 2M_s b + 2\rho wt(L - \lambda)b \quad \text{(A59)}$$

$$E = g\left[b(2M_s + M_L) + \lambda M_L + 2\rho\, wtbL + wt\ (\lambda - b)^2\right] \quad \text{(A60)}$$

Solution of the First and Second Linearized Equations of Motion

Differentiating the first equation with respect to time:

$$\ddot{x}_p = \frac{B}{A}\ \ddot{\theta}$$

Substituting $\ddot{x}_p$ into the second equation, the following equation in θ is obtained

$$\ddot{\theta} + \left[\frac{E}{C - \frac{BD}{A}}\right]\theta = 0 \quad \text{(A61)}$$

From physical considerations, it is evident that θ will be a periodic function, and therefore the solution of the above equation will be sinusoidal.

Using the initial conditions

$$\theta = 0 \quad \text{at} \quad t = 0$$

$$\theta = a \sin pt$$

where

$$p = \sqrt{\frac{E}{C - \frac{BD}{A}}} \quad \text{(A62)}$$

The period of motion will be

$$T = \frac{2\pi}{p}$$

Now that the motion of θ is known, the motion of the air pad can be derived. Remembering that $\ddot{x}_p = -\frac{B}{A}\ddot{\theta}$ and making the substitution for $\ddot{\theta}$

$$\ddot{x}_p = \frac{Ba}{A} p^2 \sin pt \tag{A63}$$

Using the following initial conditions

$$\dot{x}_p = v_0 \quad \text{at} \quad t = 0$$

$$x_p = 0 \quad \text{at} \quad t = 0$$

and integrating twice with respect to time, the following equation for x_p is obtained:

$$x_p = -\frac{Ba}{A} \sin pt + \left(v_O + \frac{BaP}{A}\right)t \tag{A64}$$

It is observed that the frequency of oscillation for both x_p and θ is the same. The amplitude of x_p, however, will be $\frac{B}{A}$ times greater than the amplitude of θ.

It should be stressed that these derived functions are only as valid as the linearization assumptions. If they do have any physical relationship to the real system, it will be for very short periods of time and small motions.

The Third Equation of Motion and Its Solution

By imposing the following limitations and assumptions, the third equation of motion can be linearized.

θ - is limited to small angles

$\dot{\theta}$ - is small

$\ddot{x}_p$ - is small

R - is constant

The assumption that the outer radius of the coiled portion of the negator spring, R, is constant is a good one since the negator spring is very thin. As a direct consequence of this assumption, the moment of inertia of the coiled negator spring can be written

$$I_{c\alpha} = M_c R^2 = \rho wt (L + b - \ell) R^2 \tag{A65}$$

Making the above-mentioned assumptions, the third equation of motion has the following linearized form:

$$\ddot{\ell} + C_1 \dot{\ell} + C_2 \ell + C_3 = 0 \tag{A66}$$

where the constant coefficients have the following values:

$$C_1 = \frac{2 D_m}{R^2 (2\rho wtL + M_L) + 2 I_{s\alpha}} \qquad C_2 = \frac{-(2\rho wtg)}{2\rho wtL + M_L + \frac{2 I_{s\alpha}}{R^2}}$$

$$C_3 = \frac{\left[2\rho wtbg - M_L g \quad F + \frac{\dot{\ell}}{|\dot{\ell}|} \frac{rf}{R}\right]}{2\rho wtL + M_L + \frac{2 I_{s\alpha}}{R^2}}$$

It should be noted that the coefficient C_3 changes value with a change in sign of $\dot{\ell}$. This means C_3 will have one value while the subject mass is rising and another during the fall.

When a and b are two real distinct roots of the characteristic equation $S^2 + C_1 S + C_2 = 0$, the differential equation has the following solution:

$$\ell(t) = -C_3 \left[\frac{1}{C_2} + \frac{1}{a(a-b)} e^{at} + \frac{1}{b(b-a)} e^{bt}\right]$$
$$+ \left[\dot{\ell}(0^+) + C_1 \ell(0^+)\right] \left[\frac{1}{a-b} e^{at} + \frac{1}{b-a} e^{bt}\right]$$
$$+ \ell(0^+) \left[\frac{a}{a-b} e^{at} + \frac{b}{b-a} e^{bt}\right] \tag{A67}$$

The constant D_m, which is the damping coefficient, is found to be very small for roller bearings lubricated with light oil.[1] If D_m is sufficiently small, the constant C_1 can be neglected in the differential equation. For the case where C_1 is neglected, the following equation of motion is obtained:

$$\ell(t) = \frac{C_3}{C_2} + \left[\ell(0^+) - \frac{C_3}{a^2}\right] \cosh at + \dot{\ell}(0^+) \frac{\ell}{a} \sinh at \tag{A68}$$

where $a = \left|\sqrt{-C_2}\right|$ and is real.

Differentiating with respect to time, the velocity and acceleration are calculated.

$$\dot{\ell}(t) = a\left[\ell(0^+) - \frac{C_3}{a^2}\right]\sinh at + \left[\dot{\ell}(0^+)\right]\cosh at \tag{A69}$$

$$\ddot{\ell}(t) = a^2\left[\ell(0^+) - \frac{C_3}{a^2}\right]\cosh at + a\left[\dot{\ell}(0^+)\right]\sinh at \tag{A70}$$

The time at which $\dot{\ell}(t) = 0$, which is the instant that C_3 changes value, is

$$t_p = \frac{\ell}{a}\tanh^{-1}\frac{-\dot{\ell}(0^+)}{a\left[\ell(0^+) - \frac{C_3}{a^2}\right]} \tag{A71}$$

where C_3 is evaluated at t_p^-. It can also be shown that the acceleration $\ddot{\ell}$ will have a minimum at the time t_p.

For the purpose of judging the performance of this lunar gravity simulator, $\ddot{\ell}(t)$ should be investigated. For good simulation, this acceleration should approximate 1/6g or the gravity on the moon.

Sample Calculations

In the following calculations, the following parametric values will be assumed:

$M_p = 1.56 \times 10^{-2}$ slugs

$M_L = .558$ slugs

$M_h = 3 \times 10^{-3}$ slugs

$M_s = 4.5 \times 10^{-3}$ slugs

$2\rho wt = 5.8 \times 10^{-4}$ slugs/in.

$\rho = .00879$ slugs/in.^{3}

$w = 1.5$ in.

$t = .022$ in.

$R = 1.75$ in.

$L = 144$ in.

$\lambda = 120$ in.

$b = 1.80$ in.

$I_{s\alpha}$ = .0208 slug-in.^{2}

$I_{h\theta}$ = 9.7×10^{-3} slugs-in.^{2}

$I_{s\theta}$ = 14.6×10^{-3} slugs-in.^{2}

D_m = 3.2×10^{-7} in.-lb-sec

τ_f = .010 in./lb

g = 32.2 ft/sec^2

Calculation of Up-and-Down Motion

For the purpose of this calculation, a subject mass of .558 slugs was chosen. This mass will have an earth weight of 18 pounds. As a first attempt at designing a simulator, negator spring force of 15 pounds is chosen. With this spring force, almost 5/6 of the subject mass's earth weight will be negated statically.

The subject mass is now given an initial velocity upward and its motion is observed. The initial conditions are

$$\ell(0^+) = 120 \text{ in.}$$

$$\dot{\ell}(0^+) = -88 \text{ in./sec}$$

then

$$C_2 = -.342 \text{ sec}^{-2}$$

$$C_3 = -54.1 \text{ in./sec}^2$$

$$a = -.5845 \text{ sec}^{-1}$$

Due to the fact that the damping coefficient D_m is very small, C_1 can be neglected and the following equation applies

$$\ell(t) = -\frac{C_3}{C_2} + \left[\ell(0^+) - \frac{C_3}{a^2}\right] \cosh at + \dot{\ell}(0^+) \frac{\ell}{a} \sinh at$$

The rise in time is found to be t = 1.032 sec. At this time the subject mass will have zero velocity and a distance 1 of 76.3 in., which corresponds to a lump height of 43.7 in.. For the fall, the value of C_3 will change due to the influence that the change in direction of velocity has upon the friction in the bearing. The new constant is C_3 = -54.5 in./sec^2. The drop time is then found to be t = 1.032 sec.

In general, the drop and rise times will not be the same. However, under this set of conditions, there is negligible difference between them.

The height above the floor and the acceleration of the subject mass for this jump are shown plotted versus time in Figures A2 and A3 respectively. For the purpose of comparison, the values of height and acceleration for a jump on the moon under the same initial conditions are also plotted.

It is evident from these graphs that the simulation is far from perfect. Namely, the jump height on the simulator is 43.7 in. compared to 59.9 in. on the moon. In addition, the acceleration is still much higher than the lunar acceleration. It can be concluded from this that the choice of a 15-pound negator spring which will give good static simulation is not adequate dynamically.

To demonstrate this point, a new negator spring force of 15.8 lb is chosen. The height and acceleration versus time curves for this spring force are also plotted on Figures A2 and A3. As can be seen, the simulation is greatly improved, but as would be expected, still not perfect. It is important to note that the acceleration has an almost hyperbolic shape rather than being constant.

Calculation of Oscillatory Motion

Keeping in mind the large number of restrictions necessary for the solution of the first and second equations of motion, the following analysis is presented.

Solving the equations derived in the section on the third equation of motion for θ and x_p about the operating point $\lambda = 120$ in., the following is obtained:

The angular frequency $p = 2.12$ rad/sec

The period $T = 2.96$ sec

and the equations for θ and x_p are

$$\theta = a \sin (2.12t)$$

$$x_p = -31.8a \sin (2.12t) + (67.4a + V_o)\, t$$

Recalling that the total jump time for the 15.8 lb negator spring was 2.64 seconds, it is evident that, if the above equations have any physical significance, it will be only for a very small portion of the total period.

Conclusion

The equations of motion of a lunar gravity simulator were derived using the method of Lagrange. These equations were found to be highly nonlinear; and, therefore, an attempt was made to linearize them. Some of the assumptions necessary for the linearization are of a questionable nature. This fact must be kept in mind when reviewing the results of these equations.

It was found that, for the up-and-down motion of the subject mass, a negator spring force which would give good static lunar simulation would not yield good dynamic characteristics. It was also found that by adjusting the negator spring force to a higher level, the dynamic characteristics could be improved.

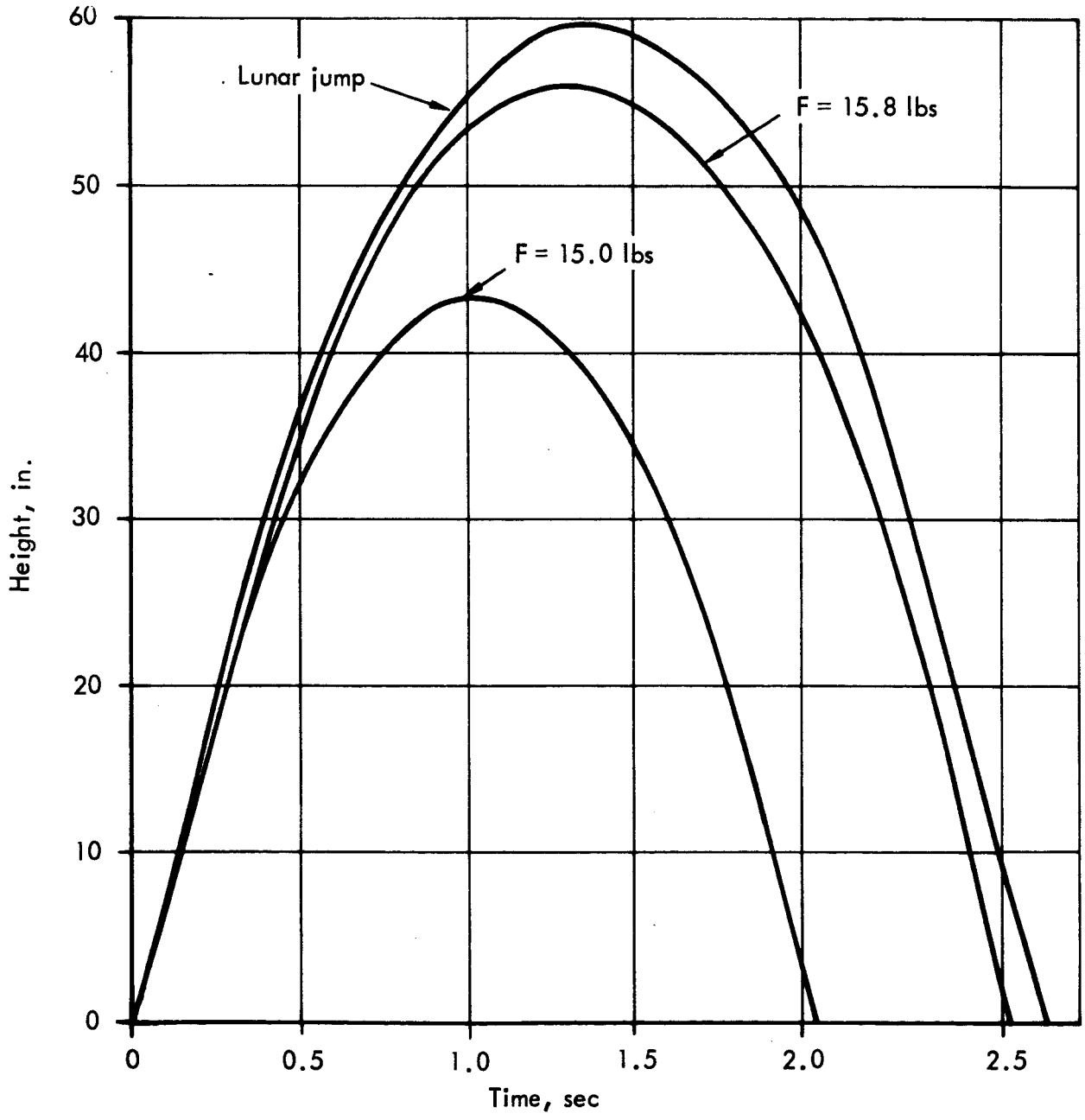

Figure A2. - Comparison of height vs. time curves for an initial velocity of 88 in./sec

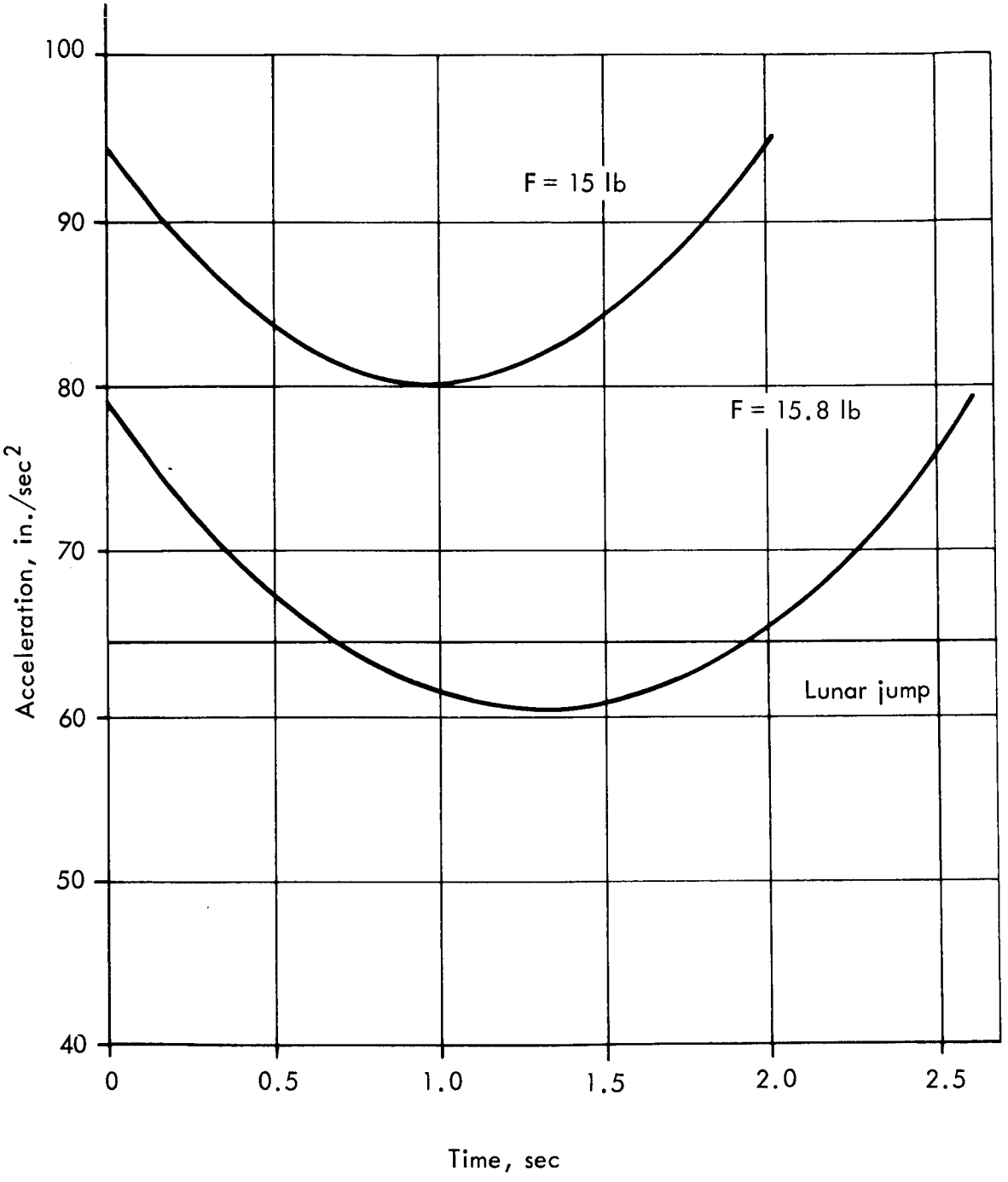

Figure A3. - Comparison of acceleration vs. time curves for an initial velocity of 88 in./sec

Recalling that it is possible to obtain negator springs with a positive force gradient, it is probable that such a spring would flatten out the acceleration versus time curve for a jump and therefore improve the dynamic simulation.

The influence of a positive force gradient negator spring and the possibility of numerical solutions to the nonlinear differential equations will be the objects of future work.